EES Catalysis

MINIREVIEW

View Article Online
View Journal | View Issue

Cite this: *EES Catal.*, 2023, 1, 687

A review of II–VI semiconductor nanoclusters for photocatalytic CO_2 conversion: synthesis, characterization, and mechanisms

Kai Li,†[a] Junjun Ge,†[b] Enhao Li,[b] Zhe Li,[b] Hua Wang,[d] Yuanyuan Wang, *[b] Yang Zhou*[c] and Jun-Jie Zhu *[b]

Received 16th May 2023,
Accepted 14th June 2023

DOI: 10.1039/d3ey00106g

rsc.li/eescatalysis

The excessive consumption of fossil fuels has caused a severe energy shortage, and the large amount of CO_2 released during the combustion process has disrupted the carbon balance in nature. Achieving photocatalytic CO_2 reduction to high-value products is of high significance for both the economy and environment. So far, the bottlenecks for photocatalytic reduction of CO_2 include low electron–hole separation efficiency and low CO_2 productivity. II–VI semiconductor nanoclusters, especially magic-size clusters (MSCs), possess special chemical and physical properties such as an adjustable band gap (broadening the spectral response range), short carrier migration distance (favoring charge separation), and high surface-to-volume ratio (providing more active sites for CO_2 adsorption and conversion), making them potent candidates for photocatalysis. This review briefly introduces the research progress in II–VI MSCs. Then, we summarize the recent advances in II–VI MSCs and related composites for photocatalytic CO_2 reduction. Finally, the challenges and prospects of MSC-based photoelectron-catalytic systems are also discussed.

Broader context

In recent years, photocatalytic CO_2 conversion has attracted great interest, as it exhibits great theoretical value and application prospects. Notably, proper band structure, wide spectrum responsiveness, high affinity towards CO_2 molecules, and high stability during the photocatalytic process are necessities for an ideal semiconductor photocatalyst to conduct photoconversion of CO_2 with high efficiency. Besides these, a high turnover frequency of CO_2 as well as high selectivity for the products are also crucial for its potential industrial application. However, it is difficult for traditional semiconductor nanostructures to possess all the advantages mentioned above, especially those comprised by single components. Fortunately, seeking innovation in materials is an effective pathway to break through the current bottleneck faced by photocatalytic CO_2 reduction, in which II–VI "magic-size" clusters (MSCs) are one of the high-potential candidates. Theoretically, their tunable direct band gaps, short carrier migration distance, and high specific surface area make possible a highly efficient charge separation under a broad spectral irradiation, while providing sufficient active sites for the adsorption and activation of CO_2; thus, they are expected to exhibit significantly enhanced photocatalytic performance in comparison with their larger-sized counterparts. Currently, the rational design, controllable synthesis, and precise modification of II–IV MSCs with customized photoelectron performance can be realized, which is attributed to the continuously deepening understanding of their growth mechanism with the assistance of various of *in situ* characterization techniques. However, studies on their photocatalytic performance for CO_2 conversion are still in the computational simulation stage, with little experimental progress reported. Therefore, in this review, we briefly overview the syntheses, compositions, growth mechanisms, *in situ* characterization, and performance improvement strategies of typical II–VI MSCs. Next, recent advances on the application of II–VI MSCs for photocatalytic CO_2 reduction are introduced. Although there are still few reports on the relevant experimental progress, computational simulations predict the feasibility and bright future of MSCs in this field. Finally, the current challenges and future prospects of MSC-based photoelectron catalytic systems are also discussed.

[a] *School of Science, Wuhan University of Science and Technology, Wuhan 430065, P. R. China*
[b] *State Key Laboratory of Analytical Chemistry for Life Science, School of Chemistry and Chemical Engineering, Nanjing University, Nanjing 210023, China. E-mail: wangyy@nju.edu.cn, jjzhu@nju.edu.cn*
[c] *Key Laboratory for Organic Electronics & Information Displays (KLOEID), Institute of Advanced Materials (IAM), Nanjing University of Posts & Telecommunications (NJUPT), Nanjing 210046, China. E-mail: iamyangzhou@njupt.edu.cn*
[d] *Huzhou Key Laboratory of Medical and Environmental Applications Technologies, School of Life Sciences, Huzhou University, Zhejiang 313000, P. R. China*
† These authors contributed equally.

1. Introduction

As the main factor disrupting the natural carbon balance and causing global warming, excessive CO_2 emission from fossil fuel combustion is of particular concern.[1–3] Converting CO_2 into high-value-added fuels, chemicals, and other target compounds is not only a potential negative carbon emission strategy, but also an effective approach for the resourceful

use of CO_2, which is consistent with the concept of green and sustainable development.[4–8] In recent years, photocatalytic CO_2 conversion has aroused great interest, exhibiting great theoretical value and application prospects.[9–12] Generally, an ideal material for photocatalytic CO_2 conversion should be stable and able to respond to a wide range of solar spectra for the generation of photoinduced electron–hole pairs with high efficiency.[9,12,13] In addition, a high turnover frequency towards CO_2 and high selectivity for the products are also crucial, as this determines whether photocatalytic CO_2 reduction has the potential for industrial application.[13–15]

II–VI semiconductors with tunable direct band gaps have inherent advantages in designing and constructing high-performance photocatalysts.[16–18] Among them, the II–VI magic-size clusters (II–VI MSCs), which are series of semiconductor nanoclusters composed of tens to hundreds of atoms from groups II (such as Zn, Cd, *etc.*) and VI (such as S and Se, *etc.*), with diameters ranging from 1 to 10 nanometers, are potential candidates for efficient photocatalytic CO_2 conversion due to their high specific surface area, adjustable surface ligands, and excellent photoelectric performance.[19–21] In Liu *et al.*'s research,[22] magic-size $(CdSe)_{13}$ was stored at room temperature for a whole year to evaluate its stability. They found that $(CdSe)_{13}$ displayed better thermodynamic stability in comparison with other MSCs, and its morphology was maintained during the storage tests without any aggregation or decomposition. Besides, the band gap of CdSe nanoclusters can be accurately adjusted according to their size and surface ligand properties, thereby meeting the requirements of wide spectral responsiveness.[23] Moreover, the small size and large specific surface area of semiconductor nanoclusters contribute to the exposure of catalytic active sites, making it easier for the combination and conversion of reactant molecules. Compared to the corresponding bulk materials, the average migration distance of photogenerated electron–hole pairs to the surface of MSCs is significantly shortened, which reduces their matrix recombination and increases the probability for them to initiate photoinduced redox reactions. Therefore, MSCs are very promising for the construction of photocatalytic systems with high performance, and they have met success in some pioneering works.[24,25]

However, there are still several challenges to using II–VI MSCs for photocatalytic CO_2 conversion. On the one hand, the high dissociation energy of C=O in CO_2 (about 750 kJ mol^{-1}) means that improving the activation ability of MSCs for CO_2 molecules is crucial to enabling efficient photocatalytic reactions over a wide spectral range.[26] On the other hand, the tunable band structure of MSCs still needs to be optimized to make the conductive band (CB) more negative than the reduction potential of CO_2, as shown in Table 1.[27] The stability of MSCs in the appropriate solvent for CO_2 is another key point that contributes to the adsorption and conversion of CO_2 on their surface. Using MSCs as a cocatalyst to construct a composite photocatalytic system could be a promising solution.[28–31] Recently, research on II–VI nanostructure (nanoplates, nanoparticles, quantum dots, *etc.*)-involved heterojunctions for photocatalytic CO_2 reduction has made some progress.[28–30] It is reasonable to believe that using II–VI MSCs with clear structure, larger specific surface area, and tunable energy band as a substitute will significantly improve photocatalytic performance, although the related research is still rare.

Table 1 Electrochemical potentials of H_2O oxidation and CO_2 reduction into various products

	Reactions	E^0 (V) *vs.* NHE at pH 7
1	$2H_2O + 4h^+ \rightarrow O_2 + 4H^+$	1.23
2	$CO_2 + e^- \rightarrow CO_2^-$	−1.9
3	$CO_2 + 2H^+ + 2e^- \rightarrow CO + H_2O$	−0.53
4	$CO_2 + 2H^+ + 2e^- \rightarrow HCOOH$	−0.61
5	$CO_2 + 4H^+ + 4e^- \rightarrow HCHO + H_2O$	−0.48
6	$CO_2 + 6H^+ + 6e^- \rightarrow CH_3OH + H_2O$	−0.38
7	$CO_2 + 8H^+ + 8e^- \rightarrow CH_4 + 2H_2O$	−0.24
8	$2H^+ + 2e^- \rightarrow H_2$	−0.41

The composition, morphology, and surface ligands of MSCs can be controlled through rational design and targeted synthesis strategies, which are key factors determining their optoelectronic properties and may have significant influence on their potential photocatalytic performance. Therefore, in this review, we first briefly overview the synthesis and compositions, growth mechanisms, and performance improvement strategies of typical II–VI MSCs. Then, recent advances on the application of II–VI MSCs for photocatalytic CO_2 reduction are introduced. Although there are still few reports on the relevant experimental progress, computational simulations predict the feasibility and bright future of MSCs in this field. Finally, the current challenges and future prospects of MSC-based photoelectron-catalytic systems are also discussed.

2. Synthesis and growth mechanism of typical II–VI MSCs

Research has shown that MSCs are essential intermediates in the formation of II–VI semiconductor nanostructures, such as nanobelts, nanoribbons, and quantum dots.[32–37] As is known, these metal chalcogenide nanomaterials with great potential in the fields of optoelectronic manufacturing,[16,38,39] photo/photothermal catalysis,[17,18] and new energy[40,41] have been studied in depth and seen great progress in the past few decades. In contrast, current topics are more focused on their ultrasmall intermediates due to the quantum confinement that brings about special phenomena and significantly enhances the conventional performance.

In relevant research, the first issue that needs to be addressed is the synthesis of MSCs. Except for the isolation of existing MSCs during the formation of larger II–VI semiconductor nanostructures, direct synthesis strategies have been developed to obtain MSCs with the desired stoichiometry and make it possible to regulate and control the performance of the products.[33–37,42–44] Since the successful synthesis of $(CdSe)_{33,34}$ clusters by Kasuya *et al.* in 2004,[44] numerous direct-synthesized MSCs as well as other synthetic methodologies have been reported. Zhou and colleagues are one of the first groups to

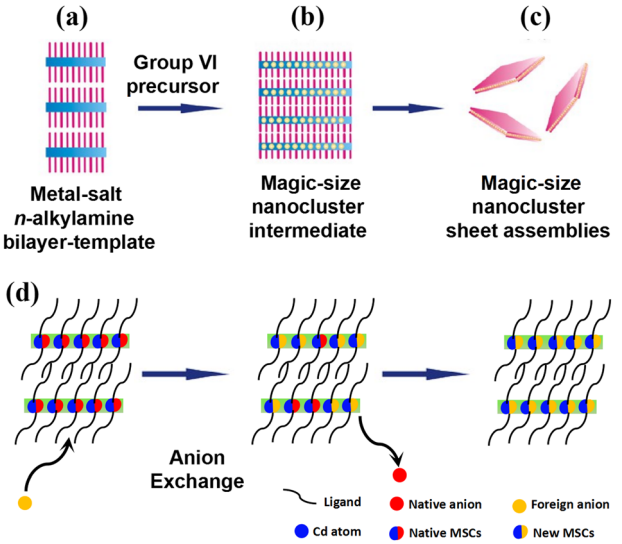

Fig. 1 (a) The combination of metal salts and primary-amine solvents forms lamellar, primary-amine-bilayer templates. (b) The addition of group VI precursors results in the growth of magic-size nanoclusters within the templates. (c) Ligand exchange with oleylamine liberates sheetlike aggregates. (d) Formation of new MSCs *via* an anion exchange pathway. Reproduced from ref. 48 and 49 with permission from the American Chemical Society.

conduct the synthesis and separation of II–VI semiconductor nanoclusters, pioneering the synthesis of nine II–VI "magic size" inorganic semiconductor nanoclusters.[45,46]

Among them, the strategy (see Fig. 1(a)–(c)) proposed by Buhro *et al.* is regarded as a universal one for the synthesis of most $(ME)_n$ clusters (M: metal, E: chalcogenide).[47,48] Typically, a metal-salt primary-amine bilayer is formed firstly as a template. After adding chalcogenide precursor into the reaction system, $(ME)_n$ cluster is generated and released from templates due to the ligand-exchange-induced unbundling process. On this basis, the as-obtained $(CdS)_{13}$ MSCs could act as a single precursor to form colloidal CdS nanoplatelets with a wurtzite structure.[49] In addition, Yu *et al.*[50] demonstrated for the first time how colloidal semiconductor MSCs undergo isomerization at low temperatures under external chemical stimuli, namely, MSC-399 to MSC-422. Notably, ion exchange makes it possible for as-obtained MSCs to transform into their counterparts, indicating that new MSCs can be synthesized *via* a template-based approach (see Fig. 1(d)).

Precursor compounds (PCs) also play a vital role in the formation of MSCs. As reported by Yang *et al.*, two different MSCs (MSC-299 and MSC-328) were transformed from ZnSe PCs by introducing octylamine and acetic acid into the reaction system at room temperature. Their study proposes the composition of PCs for the first time (ZnSe PCs with a formula of $Zn_{16}Se_{32}$) and determines the formation of the covalent bond Zn–Se in ZnSe PCs, therefore deepening the understanding of the transformation relationship between PCs and MSCs and providing a new path for the synthesis of MSCs. In addition, diphenylphosphine (DPP) can inhibit the decomposition of Zn precursors and reduce the generation of by-products, which is also considered to play a crucial role in the synthesis of other PCs and related MSCs.

It is worth noting that MSCs with special stability always require "jumps" to obtain a series of crystallites with no intermediate sizes. In order to further clarify the growth mechanism of MSCs, nine magic-sized CdSe clusters with increased sizes were synthesized by Mule and coworkers, together with the proposition of a microscopic model based on classical nucleation theory.[34] Results show that these nanocrystals grow layer by layer from one size to the next-larger size sequentially, which could be ascribed to the synergism of size-dependent nanoscale effects and the tetrahedral shape, while the surface-reaction-limited conditions take charge. Although this study only focuses on the growth of CdSe MSCs, the general growth mechanism is valuable for the study of related II–VI semiconductor MSCs and can provide guidance for their synthesis.

3. *In situ* characterization of typical II–VI MSCs

As is known, traditional non-*in situ* characterization techniques require a certain pre-treatment procedure for the test samples to meet testing requirements. During the process, some important information about their morphology, structure, as well as surface properties may be lost. Moreover, the detection of reaction intermediates is difficult to achieve using non-*in situ* characterization techniques. Therefore, researchers have turned to *in situ* characterization techniques for assistance, in order to monitor the reaction process in real time and speculate on the possible reaction mechanism by analyzing the intermediates in each stage of the reaction. To date, *in situ* characterization technologies run through the synthesis, separation, and performance evaluation of MSCs to determine their composition, structure, and physicochemical properties, while avoiding damage to them during the above process. Typically, time-of-flight mass spectrometry (TOF-MS) can provide exact information about the molecular mass and possible structures of MSCs by relating the molecular mass and the isotope patterns, which also helps to elucidate the formation mechanism of specific MSCs. As reported by Kasuya *et al.*, highly stable mass-to-charge ratios (m/z) related to $(CdSe)_{33}$ and $(CdSe)_{34}$ were obtained by using laser desorption ionization mass spectroscopy (LDI-MS).[44] Meanwhile, the detachment of surface ligands in MSCs during the ionization process is of great significance for studying the surface properties of MSCs, which has significant impacts on their photoelectric performance.[51–53] In addition, this relatively mature technique also contributes to determining the mesostructures formed by the assembly of MSCs.[54]

On this basis, more information about the core and shell of MSCs can be obtained using nuclear magnetic resonance (NMR) technologies.[55–57] According to Li's research, different Cd atoms (in the core or on the surface) can be differentiated by

Table 2 Study on the composition, structure, and surface properties of MSCs using *in situ* characterization techniques

Methods	Research object	Applications	Ref.
TOF-MS	Study the molecular mass, possible structures, surface ligands, growth pathways of MSCs	Obtaining highly stable mass-to-charge ratios (m/z) related to $(CdSe)_{33}$ and $(CdSe)_{34}$	44 and 51–54
NMR	Investigate the inorganic core and organic shell (ligands) of MSCs	Distinguishing ^{113}Cd atoms in the core or on the surface of $(CdSe)_{13}$	55–57
SAXS	Analyze the crystal structure, size and shape, and growth pathways (intermediates and mesophases) of MSCs	Demonstrating the presence of intermediates formed during the induction period of CdTe MSCs	58–60
EXAFS	Monitor the structural changes of MSCs induced by different capping ligands	Discovering the relationship between Cd–S distance in CdS MSCs and their surface ligands (longer for thiol capping ligands, shorter for polyphosphonate capping ligands)	61

comparing the ^{113}Cd cross-polarization magic-angle spinning (CP-MAS) and ^{113}Cd MAS NMR spectra.[57]

The structure of MSCs is another current focus that can be determined by small-angle X-ray scattering (SAXS). Benefiting from the well-defined peaks, SAXS not only can characterize the crystal structure of MSCs but also demonstrate the existence of intermediates and mesophases during their formation, further elucidating their growth pathways.[58,59] Moreover, the local environment, especially the structural changes induced by different capping ligands, can be investigated by extended X-ray absorption fine structure spectroscopy (EXAFS).[60]

Obviously, through a series of *in situ* characterization techniques, the composition, structure, size, surface state, and growth mechanism of MSCs have been clearly revealed (see Table 2), providing valuable information for their future targeted design and modification to meet the needs of photocatalytic CO_2 reduction.

4. Modification on typical II–VI MSCs for enhanced performance

Doping or alloying can provide additional assistance for the property modulation and enhancement of MSCs, although it is more challenging to obtain MSCs with controlled amount of dopant, as compared to implementing the technique on larger semiconductor nanostructures.[61–63] As reported by Hyeon, $Mn_xCd_{13-x}Se_{13}$ nanoclusters (x = 0–2) with bright-orange photoluminescence (an evidence of Mn^{2+} doping) were synthesized by taking a modified procedure applied for preparing the Mn^{2+}-doped CdSe nanoribbons.[62] The systemic introduction of Mn^{2+} with controllable amount endows the production of MSCs with unique magneto-optical characteristics. This scalable method can also guide the synthesis of $Co_xCd_{13-x}Se_{13}$ nanoclusters (x = 0–2), although there is a significant mismatch in the radii of Co^{2+} and Cd^{2+}.[63] Notably, ion exchange makes it possible for as-obtained MSCs to transform into their counterparts, indicating that new MSCs can be synthesized *via* a template-based approach (see Fig. 1(d)). White *et al.* found that reorganization of the Cd^{2+} sublattice in $(CdSe)_{33,34}$ initiated by Cu^+ doping (treating with tetrakis(acetonitrile) copper(I) hexafluorophosphate ($[(CH_3CN)_4C\text{-}u]PF_6$) in an oxygen-free and moisture-free glove box) created a meta-stable six-coordinate structure.[64] The stronger affinity between this new structure and Cu^+ ensured continuous cation exchange, thereby successfully converting $(CdSe)_{33,34}$ into Cu_2Se for the first time. As reported by T. Hyeon,[65] the CO_2 cycloaddition reaction (from propylene oxide to propylene carbonate) catalyzed by Mn^{2+}:$(Cd_{0.5}Zn_{0.5}Se)_{13}$ MSCs suprastructures has a conversion rate of up to 95%. This new insight into the dynamics of ion exchange at the solid–liquid interface is a good supplement to the doping strategy, providing new ideas for the introduction of dopants into the MSC matrix with an accurate amount.

It should be pointed out that all the synthesis, modification, and performance improvement strategies mentioned above serve the potential applications of MSCs. Based on the scope

of this review, we will focus on the application of MSCs in the field of photocatalysis in the next section.

5. II–VI MSCs for photocatalytic CO_2 reduction

As mentioned earlier, the shorter carrier migration distance in MSCs increases the probability of photogenerated electron–hole pairs transferring to the surface of the nanoclusters. On this basis, the charge separation efficiency of MSCs can be further improved by constructing heterostructures, thereby enhancing the photocatalytic performance of the nanocomposite. According to Choudhuri's calculations, encapsulating the CdSe nanocluster (Cd_6Se_6) in NU-1000 (a metal–organic framework, MOF) allows the direct transfer of electrons (generated in the highest occupied crystal orbital [HOCO] on the linker of NU-1000 under visible light irradiation) to the lowest unoccupied crystal orbital (LUCO) of Cd_6Se_6 (see Fig. 2), leading to effective charge separation and longer lifetime of the excited state, which is beneficial for photocatalytic reactions.[66] Another important challenge faced by the chemical conversion of CO_2 is the activation process. Since structural irregularity at the atomic scale may endow small anionic metal clusters (M_n^-) with superior catalytic performance, theoretical research was conducted by Lim *et al.* to investigate the anionic activation of CO_2 on these tiny nanostructures.[67] Results based on density functional theory show that activated complexes $(M_n–CO_2)^-$ were produced by the magic-numbered Cu, Ag, and Au clusters with 1, 2, and 6 atoms. Owing to the formation of M–C bond between M_n^- and CO_2 that is partially covalent, completely delocalized electrons were transferred from the HOMO of M_n^- to the LUMO of CO_2, resulting in the chemical activation of CO_2. Obviously, with the deepening of research on the synthesis of doped or alloyed MSCs through ion exchange, it is reasonable to believe that this strategy can effectively introduce the abovementioned metal species into MSCs to enhance their adsorption and activation ability for CO_2, thus laying the foundation for high-performance photocatalytic CO_2 reduction. On this basis, a concept for efficiently selective reduction of CO_2 to CH_3OH by the ternary composites ($Cu_N/MoS_2/Ag(111)$, N = 1–8) was theoretically established, demonstrating the feasibility of MSC-included systems to convert CO_2 into value-added chemicals.[68]

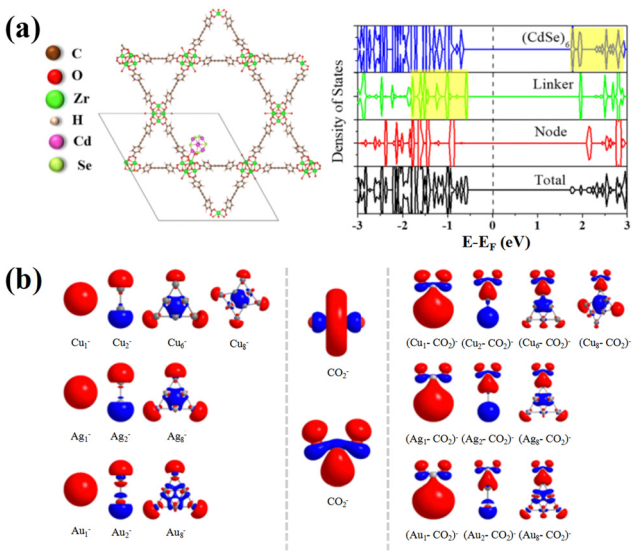

Fig. 2 (a) Structure of the Cd_6Se_6 cluster encapsulated in NU-1000 at a node site (Cd_6Se_6@NU-1000); total and partial density of states of Cd_6Se_6@NU-1000. (b) HOMOs of M_n^- clusters, LUMO of CO_2 (top) and HOMO of CO_2^- (bottom), and HOMOs of $(M_n–CO_2)^-$ complexes calculated by B3LYP functional (M = Cu, Ag, Au; n = 1, 2, 6 (and 8 for Cu)). Reproduced from ref. 66 and 67 with permission from the American Chemical Society.

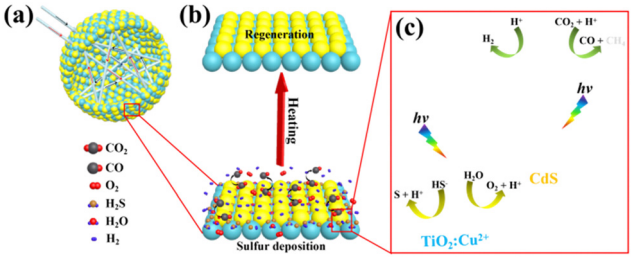

Fig. 3 (a) The complex scattering of light in the CdS/TiO_2:Cu (CTC) hollow spheres. (b) Regeneration of the catalyst by heat treatment desulfurization. (c) The step-scheme charge transfer diagram between CdS and TiO_2:Cu, as well as the redox reactions of the gaseous adsorbates under the full spectrum of xenon lamp. Reproduced from ref. 24 with permission from Wiley-VCH.

It is worth noting that although theoretical simulations predict the potential of MSCs in photocatalytic CO_2 reduction, there are still few reports on the relevant experimental progress. Fortunately, recent advances on the conventional II–VI semiconductor nanostructures for photocatalytic CO_2 reduction have great reference significance.[28–31,41] In our recent work, CdS/TiO_2:Cu hollow spheres were constructed for photocatalytic CO_2 reduction with the assistance of H_2S (see Fig. 3). The relatively high generation rates of CO (781.3 μmol g^{-1} h^{-1}) and H_2 (5875.1 μmol g^{-1} h^{-1}) indicate the high performance of the nanocomposite in the synergistic conversion of these two environmental hazards, as well as the huge potential for syngas production. Considering the enormous advantages of MSCs, it is highly anticipated that they can replace traditional II–VI nanostructures to achieve significantly enhanced performance in photocatalytic CO_2 reduction.

6. Conclusions

The advancement of synthesis and isolation methods, combined with modern characterization techniques, has given a deeper understanding of the composition, structure, and optoelectronic properties of II–VI MSCs. Moreover, the determination of growth mechanisms makes possible the rational design, controllable synthesis, and precise modification of II–VI MSCs

with customized performance. On this basis, the potential application of II–VI MSCs as a highly efficient photocatalyst was developed.

In view of the increasingly severe energy and environmental crises, as well as the steady progress of carbon peaking and carbon neutrality goals, it seems that the use of II–VI MSCs for photocatalytic CO_2 conversion can give full play to its advantages. In our opinion, progress still needs to be made in the following aspects before this can be realized:

(1) A comprehensive consideration of various factors, such as mass production of high-purity MSCs, regulation of their spectral response range, stability in CO_2-rich media, adsorption and activation capacity of CO_2, and product selectivity is in great demand, which also points to the lack of experimental verification at this stage.

(2) It is worth noting that the main product of photocatalytic CO_2 reduction now is still CO. Since C–C coupling starting with CO is relatively mature during the electrocatalytic process, combining photocatalysis and electrocatalysis to construct an optoelectronic coupling cathode (realizing the cascade of photocatalytic CO_2 reduction by II–VI MSCs and electrocatalytic C–C coupling by noble metals or Cu) to achieve the conversion of CO_2 to high-value multicarbon compounds is extremely attractive.[69–73]

(3) Combining the cathode with a high-efficiency photo anode to construct an all-light (solar)-driven self-biasing catalytic system, in which green and efficient CO_2 conversion without conventional energy consumption can be realized, is expected to become the ultimate goal in this field.[74,75]

It is worth noting that there are still many challenges to using II–VI MSCs for photocatalytic CO_2 reduction and constructing efficient CO_2 conversion systems driven by all-solar energy. However, with the continuous improvement of theoretical simulations, it is reasonable to believe that breakthroughs in related experimental research will be made in the near future. We hope that this review can inspire some constructive ideas and provide practical guidance and assistance for related work.

Author contributions

J. Ge, E. Li, Z. Li, H. Wang, Y. Wang, and J. Zhu provided important and constructive suggestions for this review. K. Li and J. Ge designed and wrote this review. E. Li edited the manuscript.

Conflicts of interest

There are no conflicts to declare.

Acknowledgements

This research was supported by the Natural Science Foundation of Jiangsu Province (BK20220405), National Natural Science Foundation of China (22276100, 22171132), Research Fund for Jiangsu Distinguished Professor (RK030STP22001), and Natural Science Foundation of Shandong Province (ZR20 20ZD37).

Notes and references

1 P. C. Frumhoff, R. Heede and N. Oreskes, *Clim. Change*, 2015, **132**, 157–171.
2 H. D. Matthews, N. P. Gillett, P. A. Stott and K. Zickfeld, *Nature*, 2009, **459**, 829.
3 J. Fu, P. Li, Y. Lin, H. Du, H. Liu, W. Zhu and H. Ren, *Eco-Environ. Health*, 2022, **1**, 259–279.
4 T. Gasser, C. Guivarch, K. Tachiiri, C. D. Jones and P. Ciais, *Nat. Commun.*, 2015, **6**, 7988.
5 Z. J. Wang, H. Song, H. M. Liu and J. H. Ye, *Angew. Chem., Int. Ed.*, 2020, **59**, 8016–8035.
6 S. Uden, P. Dargusch and C. Greig, *Joule*, 2021, **5**, 1956–1970.
7 J. Liu, J. Fu, Y. Zhou, W. Zhu, L. P. Jiang and Y. Lin, *Nano Lett.*, 2020, **20**(7), 4823–4828.
8 L. X. Liu, J. Fu, L. P. Jiang, J. R. Zhang, W. Zhu and Y. Lin, *ACS Appl. Mater. Interfaces*, 2019, **11**(29), 26024–26031.
9 G. Chen, G. I. N. Waterhouse, R. Shi, J. Zhao, Z. Li, L.-Z. Wu, C.-H. Tung and T. Zhang, *Angew. Chem., Int. Ed.*, 2019, **58**(49), 17528–17551.
10 Y. Zhao, G. I. N. Waterhouse, G. Chen, X. Xiong, L.-Z. Wu, C.-H. Tunga and T. Zhang, *Chem. Soc. Rev.*, 2019, **48**(7), 1972–2010.
11 A. Wagner, C. D. Sahm and E. Reisner, *Nat. Catal.*, 2020, **3**, 775–786.
12 X. Yang, K. Li, G. Wang, X. Li, P. Zhou, S. Ding, Z. Lyu, Y. C. Chang, Y. Zhou and W. Zhu, *Chem. – Eur. J.*, 2022, **28**(26), e202201881.
13 X. Li, J. Yu, M. Jaroniec and X. Chen, *Chem. Rev.*, 2019, **119**, 3962–4179.
14 S. Navarro-Jaén, M. Virginie, J. Bonin, M. Robert, R. Wojcieszak and A. Y. Khodakov, *Nat. Rev. Chem.*, 2021, **5**, 564–579.
15 S. Yoshino, A. Iwase, Y. Yamaguchi, T. M. Suzuki, T. Morikawa and A. Kudo, *J. Am. Chem. Soc.*, 2022, **144**, 2323–2332.
16 B. T. Diroll, B. Guzelturk, H. Po, C. Dabard, N. Y. Fu, L. Makke, E. Lhuillier and S. Ithurria, *Chem. Rev.*, 2023, **123**(7), 3543–3624.
17 A. Vaneski, J. Schneider, A. S. Susha and A. L. Rogach, *J. Photochem. Photobiol., C*, 2014, **19**, 52–61.
18 Q. Guo, S. G. Xia, Z. K. Xin, Y. Wang, F. Liang, X. L. Nan, Z. S. Lin, X. B. Li, C. H. Tung and L. Z. Wu, *J. Mater. Chem. A*, 2023, **11**, 3937–3941.
19 J. J. Ge, J. Liang, X. F. Chen, Y. L. Deng, P. W. Xiao, J. J. Zhu and Y. Y. Wang, *Chem. Sci.*, 2022, **13**, 11755–11763.
20 X. F. Chen, J. J. Ge, P. W. Xiao, Y. L. Deng and Y. Y. Wang, *Nano Res.*, 2023, **16**, 3387–3394.
21 A. Vartanian, *Nat. Rev. Mater.*, 2022, **7**, 596.

22 T. E. Hsieh, T. W. Yang, C. Y. Hsieh, S. J. Huang, Y. Q. Yeh, C. H. Chen, E. Y. Li and Y. H. Liu, *Chem. Mater.*, 2018, **30**, 5468–5477.
23 V. Singh, Priyanka, P. V. More, E. Hemmer, Y. K. Mishra and P. K. Khanna, *Mater. Adv.*, 2021, **2**, 1204–1228.
24 P. Wang, Q. Q. Yang, C. Xu, B. Wang, H. Wang, J. D. Zhang and Y. D. Jin, *Nano Res.*, 2022, **15**, 3106–3113.
25 R. Shi, Y. H. Cao, Y. J. Bao, Y. F. Zhao, G. I. N. Waterhouse, Z. Y. Fang, L. Z. Wu, C. H. Tung, Y. D. Yin and T. R. Zhang, *Adv. Mater.*, 2017, **29**, 7.
26 K. H. Kim, S. Kim, B. C. Moon, J. W. Choi, H. M. Jeong, Y. Kwon, S. Kwon, H. S. Choi and J. K. Kang, *J. Mater. Chem. A*, 2017, **5**, 8274–8279.
27 L. F. Wei, C. L. Yu, Q. H. Zhang, H. Liu and Y. Wang, *J. Mater. Chem. A*, 2018, **6**, 22411–22436.
28 Y. Huo, J. F. Zhang, K. Dai and C. H. Liang, *ACS Appl. Energy Mater.*, 2021, **4**, 956–968.
29 A. Li, T. Wang, C. C. Li, Z. Q. Huang, Z. B. Luo and J. L. Gong, *Angew. Chem., Int. Ed.*, 2019, **58**, 3804–3808.
30 H. Cho, W. D. Kim, K. Lee, S. Lee, G. S. Kang, H. L. Joh and D. C. Lee, *Appl. Surf. Sci.*, 2018, **429**, 2–8.
31 K. Li, Y. M. Cai, X. H. Yang, S. Wang, C. Teng, Y. Tian, Q. H. Min and W. L. Zhu, *Adv. Funct. Mater.*, 2022, **32**, 2113002.
32 Z. J. Jiang and D. F. Kelley, *ACS Nano*, 2010, **4**, 1561–1572.
33 M. S. Bootharaju, W. Baek, S. Lee, H. Chang, J. Kim and T. Hyeon, *Small*, 2021, **17**, 2002067.
34 A. S. Mule, S. Mazzotti, A. A. Rossinelli, M. Aellen, P. T. Prins, J. C. van der Bok, S. F. Solari, Y. M. Glauser, P. V. Kumar, A. Riedinger and D. J. Norris, *J. Am. Chem. Soc.*, 2021, **143**, 2037–2048.
35 Y. Kwon and S. Kim, *NPG Asia Mater.*, 2021, **13**, 37.
36 J. Zhang, X. Y. Hao, N. Rowell, T. Kreouzis, S. Han, H. S. Fan, C. C. Zhang, C. W. Hu, M. Zhang and K. Yu, *J. Phys. Chem. Lett.*, 2018, **9**, 3660–3666.
37 C. R. Luan, J. B. Tang, N. Rowell, M. Zhang, W. Huang, H. S. Fan and K. Yu, *J. Phys. Chem. Lett.*, 2019, **10**, 4345–4353.
38 K. Pal, A. Si, G. S. El-Sayyad, M. Abd Elkodous, R. Kumar, A. I. El-Batal, S. Kralj and S. Thomas, *Crit. Rev. Solid State Mater. Sci.*, 2021, **46**, 385–449.
39 M. F. Peng, Z. Wen and X. H. Sun, *Adv. Funct. Mater.*, 2023, **33**, 2211548.
40 Y. Xu, G. D. Li, R. S. Li, Y. Jing, H. Y. Zhang, X. Wang, Z. B. Du, J. H. Wu and Z. Lan, *Nano Energy*, 2022, **95**, 106973.
41 K. H. Li, X. K. Yang, Y. Lu, J. Y. Xue, S. C. Lu, J. J. Zheng, C. Chen and J. Tang, *Adv. Energy Mater.*, 2022, **12**, 2200725.
42 W. Baek, M. S. Bootharaju, K. M. Walsh, S. Lee, D. R. Gamelin and T. Hyeon, *Nat. Mater.*, 2021, **20**, 650–657.
43 X. X. Yang, M. Zhang, Q. Shen, Y. Li, C. R. Luan and K. Yu, *Nano Res.*, 2022, **15**, 465–474.
44 A. Kasuya, R. Sivamohan, Y. A. Barnakov, I. M. Dmitruk, T. Nirasawa, V. R. Romanyuk, V. Kumar, S. V. Mamykin, K. Tohji, B. Jeyadevan, K. Shinoda, T. Kudo, O. Terasaki, Z. Liu, R. V. Belosludov, V. Sundararajan and Y. Kawazoe, *Nat. Mater.*, 2004, **3**, 99–102.
45 Y. Zhou, F. D. Wang and W. E. Buhro, *J. Am. Chem. Soc.*, 2015, **137**, 15198–15208.
46 Y. Zhou, F. D. Wang and W. E. Buhro, *Chem. Mater.*, 2020, **32**, 8350–8360.
47 Y. Y. Wang, Y. H. Liu, Y. Zhang, F. D. Wang, P. J. Kowalski, H. W. Rohrs, R. A. Loomis, M. L. Gross and W. E. Buhro, *Angew. Chem., Int. Ed.*, 2012, **51**, 6154–6157.
48 Y. Y. Wang, Y. Zhou, Y. Zhang and W. E. Buhro, *Inorg. Chem.*, 2015, **54**, 1165–1177.
49 Y. L. Deng, J. Liang, X. K. Kong, P. W. Xiao, Y. Zhou and Y. Y. Wang, *Chem. Mater.*, 2023, **35**, 2463–2471.
50 Y. S. Yang, Q. Shen, C. C. Zhang, N. Rowell, M. Zhang, X. Q. Chen, C. R. Luan and K. Yu, *ACS Cent. Sci.*, 2023, **9**, 519–530.
51 Y. Wang, Y. Zhang, F. Wang, D. E. Giblin, J. Hoy, H. W. Rohrs, R. A. Loomis and W. E. Buhro, *Chem. Mater.*, 2014, **26**, 2233–2243.
52 S. Dolai, P. R. Nimmala, M. Mandal, B. B. Muhoberac, K. Dria, A. Dass and R. Sardar, *Chem. Mater.*, 2014, **26**, 1278–1285.
53 M. Li, J. Ouyang, C. I. Ratcliffe, L. Pietri, X. Wu, D. M. Leek, I. Moudrakovski, Q. Lin, B. Yang and K. Yu, *ACS Nano*, 2009, **3**, 3832–3838.
54 D. Wurmbrand, J. W. A. Fischer, R. Rosenberg and K. Boldt, *Chem. Commun.*, 2018, **54**, 7358–7361.
55 R. Wang, J. Ouyang, S. Nikolaus, L. Brestaz, M. B. Zaman, X. Wu, D. Leek, C. I. Ratcliffe and K. Yu, *Chem. Commun.*, 2009, 962–964.
56 R. Wang, C. I. Ratcliffe, X. Wu, O. Voznyy, Y. Tao and K. Yu, *J. Phys. Chem. C*, 2009, **113**, 17979–17982.
57 T. E. Hsieh, T. W. Yang, C. Y. Hsieh, S. J. Huang, Y. Q. Yeh, C. H. Chen, E. Y. Li and Y. H. Liu, *Chem. Mater.*, 2018, **30**, 5468–5477.
58 B. Abecassis, C. Bouet, C. Garnero, D. Constantin, N. Lequeux, S. Ithurria, B. Dubertret, B. R. Pauw and D. Pontoni, *Nano Lett.*, 2015, **15**, 2620–2626.
59 M. Liu, K. Wang, L. Wang, S. Han, H. Fan, N. Rowell, J. A. Ripmeester, R. Renoud, F. Bian, J. Zeng and K. Yu, *Nat. Commun.*, 2017, **8**, 15467.
60 J. Rockenberger, L. Tröger, A. Kornowski, T. Vossmeyer, A. Eychmüller, J. Feldhaus and H. Weller, *J. Phys. Chem. B*, 1997, **101**, 2691–2701.
61 J. H. Yu, X. Y. Liu, K. E. Kweon, J. Joo, J. Park, K. T. Ko, D. Lee, S. P. Shen, K. Tivakornsasithorn, J. S. Son, J. H. Park, Y. W. Kim, G. S. Hwang, M. Dobrowolska, J. K. Furdyna and T. Hyeon, *Nat. Mater.*, 2010, **9**, 47–53.
62 J. Yang, R. Fainblat, S. G. Kwon, F. Muckel, J. H. Yu, H. Terlinden, B. H. Kim, D. Iavarone, M. K. Choi, I. Y. Kim, I. Park, H. K. Hong, J. Lee, J. S. Son, Z. Lee, K. Kang, S. J. Hwang, G. Bacher and T. Hyeon, *J. Am. Chem. Soc.*, 2015, **137**, 12776–12779.
63 F. Muckel, J. Yang, S. Lorenz, W. Baek, H. Chang, T. Hyeon, G. Bacher and R. Fainblat, *ACS Nano*, 2016, **10**, 7135–7141.
64 S. L. White, P. Banerjee, I. Chakraborty and P. K. Jain, *Chem. Mater.*, 2016, **28**, 8391–8398.

65 W. Baek, M. S. Bootharaju, K. M. Walsh, S. Lee, D. R. Gamelin and T. Hyeon, *Nat. Mater.*, 2021, **20**, 650–657.
66 I. Choudhuri and D. G. Truhlar, *J. Phys. Chem. C*, 2020, **124**, 8504–8513.
67 E. Lim, J. Heo, X. X. Zhang, K. H. Bowen, S. H. Lee and S. K. Kim, *J. Phys. Chem. A*, 2021, **125**, 2243–2248.
68 Y. W. Wang, Y. D. Zhu, X. W. Zhu, J. L. Shi, X. Y. Ren, L. L. Zhang and S. F. Li, *ACS Catal.*, 2023, **13**(1), 714–724.
69 H. J. Lu, Z. L. Wang and L. Z. Wang, *ACS EST Engg.*, 2022, **2**(6), 975–988.
70 C. B. Chen, Y. F. Li, S. Yu, S. Louisia, J. B. Jin, M. F. Li, M. B. Ross and P. D. Yang, *Joule*, 2020, **4**, 1688–1699.
71 J. F. Huang, M. Mensi, E. Oveisi, V. Mantella and R. Buonsanti, *J. Am. Chem. Soc.*, 2019, **141**, 2490–2499.
72 R. Kortlever, J. Shen, K. J. P. Schouten, F. Calle-Vallejo and M. T. M. Koper, *J. Phys. Chem. Lett.*, 2015, **6**, 4073–4082.
73 S. Nitopi, E. Bertheussen, S. B. Scott, X. Y. Liu, A. K. Engstfeld, S. Horch, B. Seger, I. E. L. Stephens, K. Chan, C. Hahn, J. K. Norskov, T. F. Jaramillo and I. Chorkendorff, *Chem. Rev.*, 2019, **119**, 7610–7672.
74 V. Andrei, B. Reuillard and E. Reisner, *Nat. Mater.*, 2020, **19**, 189–194.
75 Y. J. Jang, I. Jeong, J. Lee, J. Lee, M. J. Ko and J. S. Lee, *ACS Nano*, 2016, **10**, 6980–6987.